



**Modeling Plasma Flow in Solid Propellant Charges
Using the NGEN Multiphase CFD Code**

Michael J. Nusca and Stephen L. Howard

ARL-TR-3768

April 2006

NOTICES

Disclaimers

The findings in this report are not to be construed as an official Department of the Army position unless so designated by other authorized documents.

Citation of manufacturer's or trade names does not constitute an official endorsement or approval of the use thereof.

Destroy this report when it is no longer needed. Do not return it to the originator.

Army Research Laboratory

Aberdeen Proving Ground, MD 21005-5066

ARL-TR-3768

April 2006

Modeling Plasma Flow in Solid Propellant Charges Using the NGEN Multiphase CFD Code

**Michael J. Nusca and Stephen L. Howard
Weapons and Materials Research Directorate, ARL**

REPORT DOCUMENTATION PAGE			<i>Form Approved</i> OMB No. 0704-0188	
Public reporting burden for this collection of information is estimated to average 1 hour per response, including the time for reviewing instructions, searching existing data sources, gathering and maintaining the data needed, and completing and reviewing the collection information. Send comments regarding this burden estimate or any other aspect of this collection of information, including suggestions for reducing the burden, to Department of Defense, Washington Headquarters Services, Directorate for Information Operations and Reports (0704-0188), 1215 Jefferson Davis Highway, Suite 1204, Arlington, VA 22202-4302. Respondents should be aware that notwithstanding any other provision of law, no person shall be subject to any penalty for failing to comply with a collection of information if it does not display a currently valid OMB control number. PLEASE DO NOT RETURN YOUR FORM TO THE ABOVE ADDRESS.				
1. REPORT DATE (DD-MM-YYYY) April 2006		2. REPORT TYPE Final		3. DATES COVERED (From - To) January 2005–June 2005
4. TITLE AND SUBTITLE Modeling Plasma Flow in Solid Propellant Charges Using the NGEN Multiphase CFD Code			5a. CONTRACT NUMBER	
			5b. GRANT NUMBER	
			5c. PROGRAM ELEMENT NUMBER	
6. AUTHOR(S) Michael J. Nusca and Stephen L. Howard			5d. PROJECT NUMBER 622618H8000	
			5e. TASK NUMBER	
			5f. WORK UNIT NUMBER	
7. PERFORMING ORGANIZATION NAME(S) AND ADDRESS(ES) U.S. Army Research Laboratory ATTN: AMSRD-ARL-WM-BD Aberdeen Proving Ground, MD 21005-5066			8. PERFORMING ORGANIZATION REPORT NUMBER ARL-TR-3768	
9. SPONSORING/MONITORING AGENCY NAME(S) AND ADDRESS(ES)			10. SPONSOR/MONITOR'S ACRONYM(S)	
			11. SPONSOR/MONITOR'S REPORT NUMBER(S)	
12. DISTRIBUTION/AVAILABILITY STATEMENT Approved for public release, distribution is unlimited.				
13. SUPPLEMENTARY NOTES				
14. ABSTRACT Recent requirements for hypervelocity projectile launch for strategic U.S. Army missions have led to the proposal of a variety of gun propulsion systems. Among these systems are those that utilize solid propellant along with electrothermal-chemical (ETC) augmentation. Advanced solid propellant systems with complex grain geometry and loading configuration are also being investigated. In response to this need, the U.S. Army Research Laboratory, in cooperation with Paul Gough Associates, is developing the Next Generation Interior Ballistics model, NGEN. The goal of this project is the development of an advanced interior ballistics model for use in the design and investigation of both indirect- and direct-fire gun propulsion systems. The current report demonstrates progress for application of the NGEN code to solid propellant, direct-fire gun systems in which various propellant configurations (i.e., grains and disks) are combined into a single charge in order to obtain higher-loading densities. The charge may be ignited using either a conventional (Benite) or an ETC plasma capillary. These notional charges are being investigated to determine code performance and assess the need for code upgrades, as well as to investigate propellant ignitability with Benite and plasma sources. Comparison with pressure data measured in a 25-mm ballistics simulator, filled with inert disks and grains, provides validation of the NGEN model with respect to the representation of the plasma efflux from an ablation capillary, into the chamber, and around propellant disks.				
15. SUBJECT TERMS interior ballistics, solid propellant, ignition, CFD, plasma				
16. SECURITY CLASSIFICATION OF:			17. LIMITATION OF ABSTRACT UL	18. NUMBER OF PAGES 34
a. REPORT UNCLASSIFIED	b. ABSTRACT UNCLASSIFIED	c. THIS PAGE UNCLASSIFIED		
			19b. TELEPHONE NUMBER (Include area code) 410-278-6108	

Contents

List of Figures	iv
Acknowledgments	v
1. Introduction	1
2. NGEN Code Description	2
3. Results for a Notional 120-mm Direct-Fire Charge	3
4. Results for the ARL 25-mm Simulator	8
4.1 Description of the Simulator Experiment.....	8
4.2 Description of the NGEN Code Results.....	10
4.3 Sensitivity Study for the NGEN Code Results.....	15
5. Summary and Conclusions	17
6. References	18
Distribution List	22

List of Figures

Figure 1. Electrothermal-chemical gun concept.	1
Figure 2. Diagram (dimensions in centimeters) describing propellant regions, projectile, and igniter (27).	4
Figure 3. (a) IBHVG2, XKTC, and NGEN code results for an all-granular charge ignited using Benite and (b) NGEN code results for a disk/disk/granular charge ignited using either Benite or plasma (27).....	4
Figure 4. NGEN code results (6.4 ms since igniter function) for disk/disk/grain charge ignited using Benite primer.....	5
Figure 5. NGEN code results (1.5 ms since igniter function) for disk/disk/grain charge ignited using plasma.	6
Figure 6. Current vs. time profiles used in the plasma ignition studies.....	7
Figure 7. Chamber pressure vs. time computed using the NGEN code for the disk/disk/grain charge and using the current profiles shown in figure 6.	8
Figure 8. Photographs of the ARL 25-mm simulator loaded with disks without spacers and a single Masonite disk (dimensions shown are from Chang and Howard [32]).....	9
Figure 9. Electrical profiles (current in amperes: red; power in kilowatts: green; voltage in volts: blue; and energy in joules: brown) used in the ARL 25-mm simulator tests (32).....	10
Figure 10. Pressure tap data measured in the ARL 25-mm simulator for (a) 0.015-in disk gap shown on left and (b) 0.030-in disk gap shown on right (31–33).....	10
Figure 11. Pressure tap results for a disk gap of 0.015 in: (a) data measured in the ARL 25-mm simulator shown on the left and (b) NGEN code simulation shown on the right.	11
Figure 12. Color pressure contours and superimposed velocity vectors as computed using the NGEN code for disks with a gap of 0.015 in (0.4 cm) and for times from 0.02 to 0.40 ms....	12
Figure 13. Pressure tap results for a disk gap of 0.030 in: (a) data measured in the ARL 25-mm simulator shown on the left and (b) NGEN code simulation shown on the right.	13
Figure 14. Color pressure contours and superimposed velocity vectors as computed using the NGEN code for disks with a gap of 0.030 in (0.8 cm) and for times from 0.02 to 0.40 ms....	14
Figure 15. NGEN code computed pressure results for the rear location using several levels of computational mesh resolution: (a) 0.015-in disk gap and (b) 0.030-in disk gap.	16
Figure 16. NGEN code computed pressure results for the middle location using several levels of computational mesh resolution: (a) 0.015-in disk gap and (b) 0.030-in disk gap....	16
Figure 17. NGEN code computed pressure results for the forward location using several levels of computational mesh resolution: (a) 0.030-in disk gap and (b) 0.015-in disk gap....	16

Acknowledgments

The U.S. Army Research Laboratory (ARL) Plasma-Propellant Interaction work unit, led by Mr. A. Williams and Dr. R. Beyer, and the ARL Multidimensional Modeling work unit, led by Dr. M. Nusca, supported this project. Drs. M. McQuaid and J. Powell (ARL) are recognized for capillary modeling. The Department of Defense Major Shared Resources Center at ARL supplied computer time for the simulations.

INTENTIONALLY LEFT BLANK.

1. Introduction

Future military engagements will require weapons systems exhibiting improved range and accuracy. One of the technologies under investigation to achieve these goals is the electrothermal-chemical (ETC) propulsion concept, shown schematically in figure 1. In the ETC gun, energy, which is stored either in batteries or a rotating device, is converted on demand into electrically generated plasma (resulting from the ablation of polyethylene material in a capillary) that is injected into the chamber in a howitzer or gun. This plasma energy is used to ignite the chemical propulsion charge (i.e., solid propellant) as well as to enhance gun performance by taking advantage of a number of unique plasma characteristics. For example, a low density plasma jet can efficiently ignite charges of high loading density, can control propellant mass generation rates (1), can reduce propellant charge temperature sensitivity, i.e., the variation of gun performance with changing ambient temperature (2, 3), and can shorten ignition delay, i.e., the time interval between firing of the igniter and ignition of the propellant (4). Plasma igniters replace the chemical igniter and thus enhance the safety of the gun system.

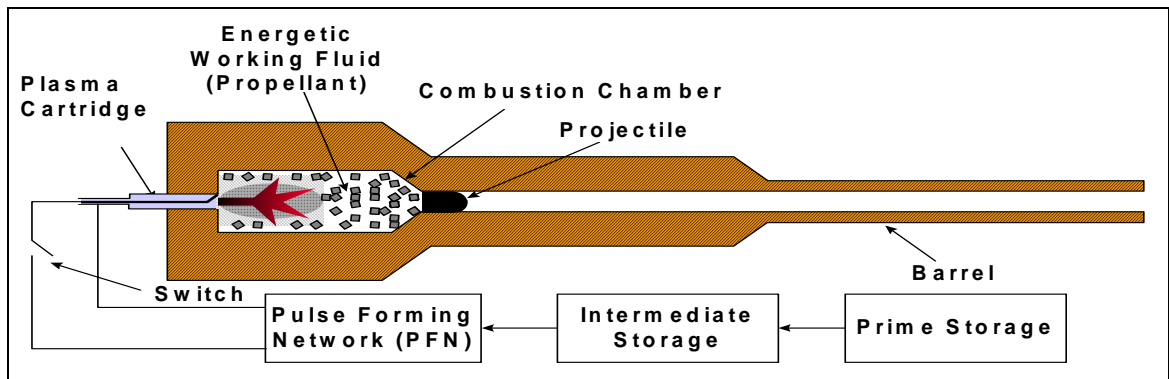


Figure 1. Electrothermal-chemical gun concept.

Research has been carried out on the use of plasmas to ignite solid propellant (5, 6). Since the plasma is at a temperature ($\sim 15,000$ K) that is higher than chemical igniters ($\sim 3,000$ K), the radiation properties of the plasma have also been considered. The high plasma temperature leads to radiation effects nearly $100\times$ greater than that of chemical igniters (i.e., a T^4 effect) (5). Such radiation could lead to significantly different temperature profiles within the propellant, causing changes in burn rates. In addition, plasma has a much lower density than the gases generated by a chemical igniter, a feature that alters the convective heat transfer to the propellant (as the plasma moves through the grains) as well as the velocity and mode of flamespreading within a propellant bed. It has been suggested that energy transport by convection may be as important as radiation transport in plasma-propellant interactions (PPIs) (7, 8).

The previously described effects can lead to significant changes in ballistic behavior and useful improvements in gun performance, but an understanding of the underlying physical mechanisms is necessary in order to achieve these goals. To this end, the U.S. Army Research Laboratory (ARL) is supporting a comprehensive study of the interaction of the plasma efflux from an ETC igniter with solid propellant. The goal of this work is to elucidate the relevant physical, mechanical, and chemical mechanisms that underlie the observed ballistic effects. Various aspects of the experimental and modeling research program for PPI are described elsewhere (9–20). The present report explores the use of a multidimensional, multiphase interior ballistics code, NGEN, that explicitly models the two-dimensional chamber geometry (including chambrage), the projectile afterbody intrusion into the chamber, the solid propellant charge, and includes the inflow of plasma into the gun chamber from an ablative polyethylene capillary. The NGEN code predicts propellant ignition and flamespreading, chamber pressurization, pressure wave travel, projectile movement, and propellant burnout. The accurate simulation of these interior ballistics parameters is important to the design of ETC guns.

2. NGEN Code Description

The U.S. Army's NGEN3 code is a multidimensional, multiphase CFD code that incorporates three-dimensional continuum equations along with auxiliary relations into a modular code structure (21–24). Since accurate charge modeling involves flowfield components of both a continuous and a discrete nature, a coupled Eulerian-Lagrangian approach is utilized. On a sufficiently small scale of resolution in both space and time, the components of the flow are represented by the balance equations for a multicomponent reacting mixture describing the conservation of mass, momentum, and energy. A macroscopic representation of the flow is adopted using these equations derived by a formal averaging technique applied to the microscopic flow. These equations require a number of constitutive laws for closure including state equations, intergranular stresses, and interphase transfer. The numerical representation of these equations as well as the numerical solution thereof is based on a finite-volume discretization and high-order accurate, conservative numerical solution schemes. The spatial values of the dependent variables at each time step are determined by a numerical integration method denoted the Continuum Flow Solver (CFS), which treats the continuous phase and certain of the discrete phases in an Eulerian fashion. The Flux-Corrected Transport scheme (25) is a suitable basis for the CFS since the method is explicit and has been shown to adapt easily to massively parallel computer systems. The discrete phases are treated by a Lagrangian formulation denoted the Large Particle Integrator (LPI), which tracks the particles explicitly and smoothes discontinuities associated with boundaries between propellants yielding a continuous distribution of porosity over the entire domain. The manner of coupling between the CFS and the LPI is through the attribution of properties (e.g., porosity and mass generation). The size of the grid as well as the number of Lagrangian particles is user prescribed.

For the simulations of novel solid propellant configurations, such as disks stacked axially along the chamber centerline and/or thin annular concentric layers (wraps), the NGEN code takes a macroscopic approach. These solid propellant media are modeled using Lagrange particles that regress, produce combustion product gases, and respond to gasdynamic and physical forces. Individual grains, sticks, slab, and wrap layers are not resolved; rather, each medium is distributed within a specified region in the gun chamber. The constitutive laws that describe interphase drag, form-function, etc., assigned to these various media, determine preferred gas flow paths through the media (e.g., radial for disks and axial for wraps) and responses of the media to forces. Media regions can be encased in impermeable boundaries that yield to gasdynamic flow after a prescribed pressure load is reached. Details of the NGEN code are supplied elsewhere (23, 24).

For modeling ETC igniters, the NGEN code has been linked to the ARL plasma capillary code developed by Powell and Zielinski (26). This capillary code uses the length, diameter, and material composition of the ablation capillary as well as the current-time profile and supplies as output the time-dependent temperature, density, molecular weight, and flow rate of the plasma efflux. This information is mapped to the computational cells that lie along the breech face of the gun chamber, from the centerline to a predetermined radial position. Pressure is linked between the NGEN code and the capillary code so that the changing chamber pressure, as computed by the NGEN code, is input the capillary code and modifies the plasma efflux. The NGEN code represents the plasma as a single component gas with properties supplied by the capillary code. Of course the plasma is actually a chemically diverse and reactive media which has been treated as such in separate modeling studies (17–19). The macroscopic approach taken in the NGEN code, with respect to plasma representation, has been used to effectively model several solid propellant charge configurations (27, 28).

3. Results for a Notional 120-mm Direct-Fire Charge

In a previous paper, Conroy and Nusca (27) used the NGEN code to simulate a modified M829 tank charge containing three regions of propellants and the M829A1 projectile (without fins) intruding into the charge (see figure 2). The solid propellant charge is JA2 and the total propellant mass is nominally the same as that of the M829A1 charge. In that study, the charge was ignited using typical parameters for a Benite primer (from a M829A1 XKTC calculation) and a typical 120MW ETC plasma capillary source (27). Comparisons of the basic charge with the Benite primer were made using both the lumped-parameter IBHVG2 (29) and one-dimensional multiphase XKTC (30) interior ballistics codes.

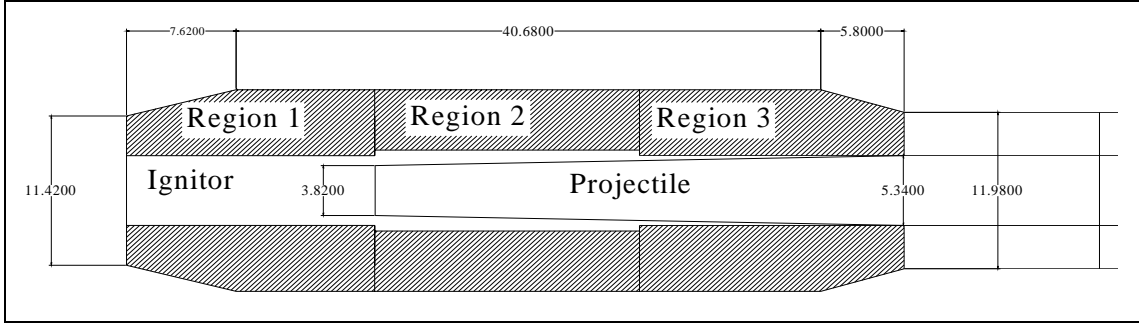


Figure 2. Diagram (dimensions in centimeters) describing propellant regions, projectile, and igniter (27).

The breech pressure-time results of the benchmark charge (i.e., 19 perf JA2 cylindrical grains in regions 1, 2, and 3 of figure 2) are shown in figure 3a. Both the XKTC and the IBHVG2 results agree, while the NGEN code calculation shows some broadening of the pressure at the peak. This discrepancy is thought to arise when the NGEN simulation allows burning propellant to become temporarily trapped beneath the chambrage and then later dislodged and allowed to flow down the tube. This charge was then modified by replacing the rear two thirds of the charge with propellant disks (i.e., regions 1 and 2 of figure 2) having the same web and total mass as the grains to investigate ignition and flame spreading issues associated with this geometry typically used in higher loading density charges. Plasma ignition for this charge was compared to ignition produced by the Benite primer. Figure 3b shows the initial pressure-time results. What is immediately evident is that the pressurization and therefore ignition is much faster with the 120MW plasma igniter as compared to the Benite primer; after a long delay, the Benite ignites the disks.

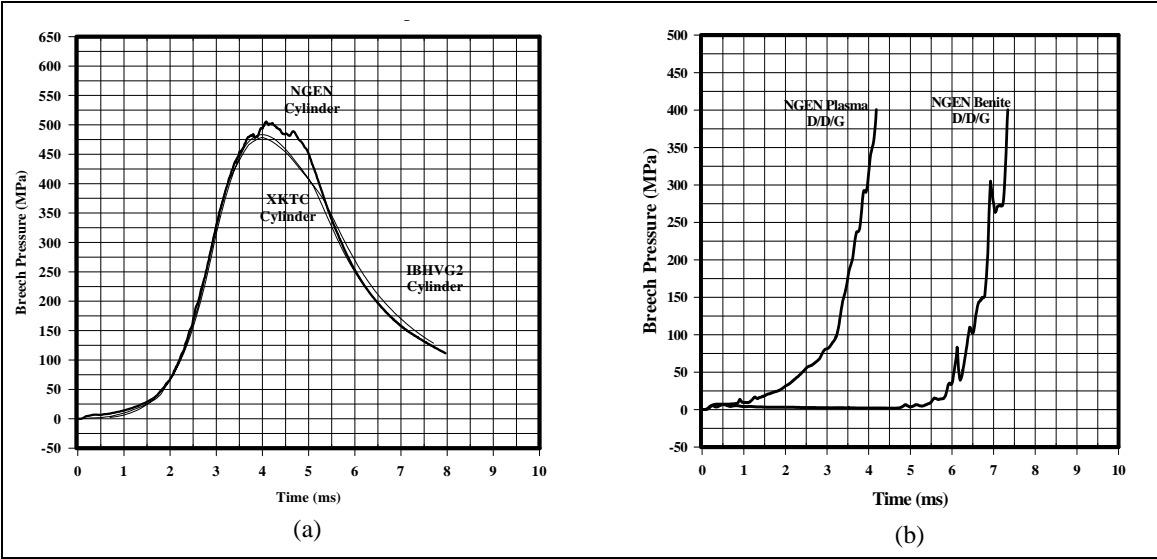


Figure 3. (a) IBHVG2, XKTC, and NGEN code results for an all-granular charge ignited using Benite and (b) NGEN code results for a disk/disk/granular charge ignited using either Benite or plasma (27).

Figure 4 shows results from the NGEN code plotted at color contours of four flow variables—porosity (blue to red, 0 to 1: open space to solid), igniter mass fraction (blue to red, 0 to 1: none to all), propellant temperature (blue to red: 294 K to 444 K), and gas pressure (blue to red: 1 to 8 MPa and above). Gas flow velocity vectors are superimposed on the propellant temperature contours. The ignition temperature of the propellant is assumed to be 444 K. The Benite igniter is assumed to be located along the centerline of the chamber from the breech wall to 15 cm. At the time of 6.4 ms, the igniter has been exhausted and igniter gas resides mainly near the chamber breech, the forward charge of granular propellant is completely ignited, causing a pressurization of the forward chamber, and a negative pressure differential (i.e., breech pressure level is below forward pressure level). Referring back to figure 3b, at this time the chamber pressure is building to the point that that full ignition is imminent. These results indicate that the long ignition delay for the disk/disk/grain charge using the Benite primer is due to the inefficient transport of igniter gases between the disks (note vertical velocity vectors up to 35 cm and above the projectile afterbody [figure 4]). This results in reduced convective heat transfer into this region.

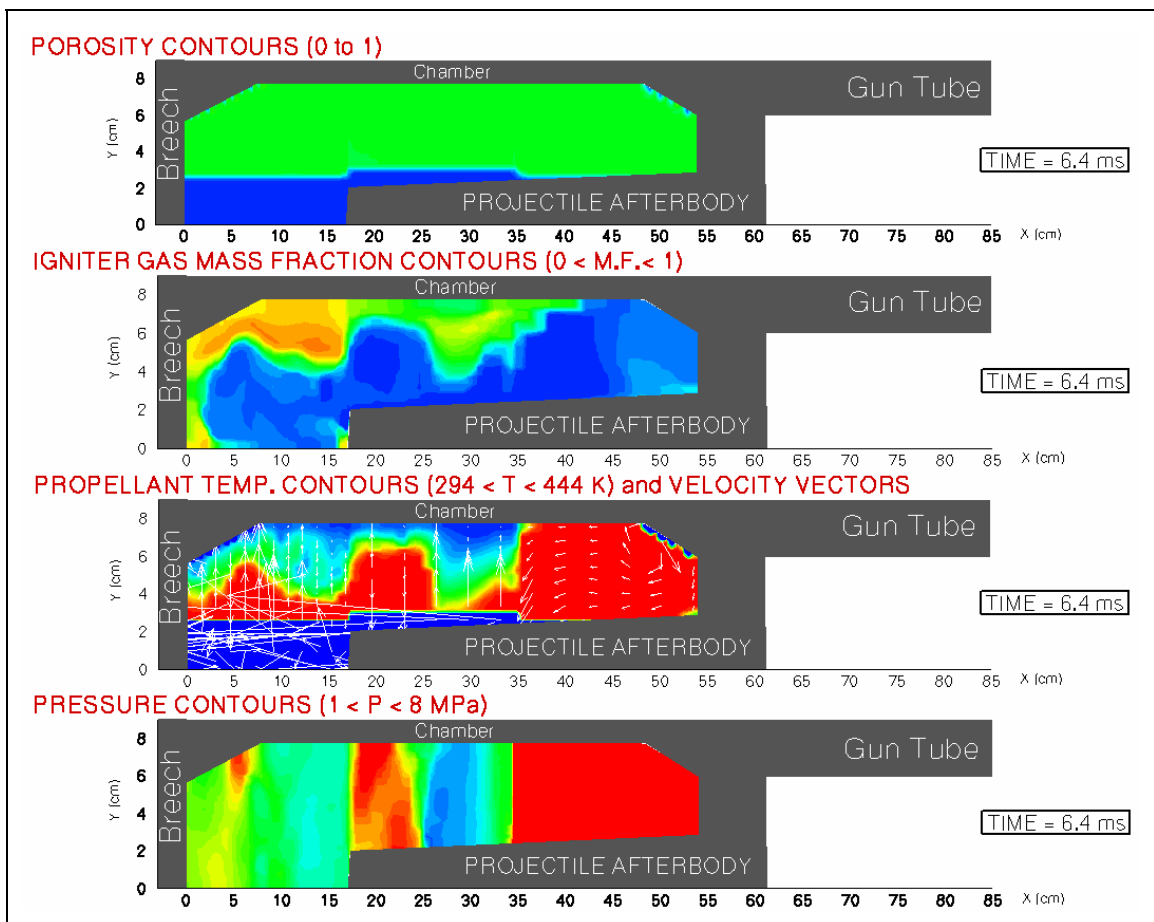


Figure 4. NGEN code results (6.4 ms since igniter function) for disk/disk/grain charge ignited using Benite primer.

Figure 5 shows results from the NGEN code plotted at color contours of four flow variables – porosity (blue to red, 0 to 1: open space to solid), plasma mass fraction (blue to red, 0 to 1: none to all), propellant temperature (blue to red: 294 K to 444 K), and gas pressure (blue to red: 1 to 8 MPa and above). Gas flow velocity vectors are superimposed on the propellant temperature contours. The ETC igniter is assumed to be located along the breech wall so that the plasma efflux issues into computational cells from the chamber centerline to 0.7 cm. At the time of 1.5 ms, the plasma has been distributed throughout the chamber, both the rear charge of propellant disks and the forward charge of propellant grains are near complete flamespread, and the favorable pressure differential (i.e., breech pressure level is above the forward pressure level) exists in the chamber. Referring back to figure 3b, at this time the chamber pressure is building to the point that that full ignition is imminent. These results indicate that the short ignition delay for the disk/disk/grain charge using a plasma igniter is due to the efficient transport of plasma between the disks and the resulting advanced progress of convective heat transfer to this region of propellant. This effect is largely due to the fact that the plasma has a molecular weight of about 4.5 as compared to the Benite gas, which is about 33.

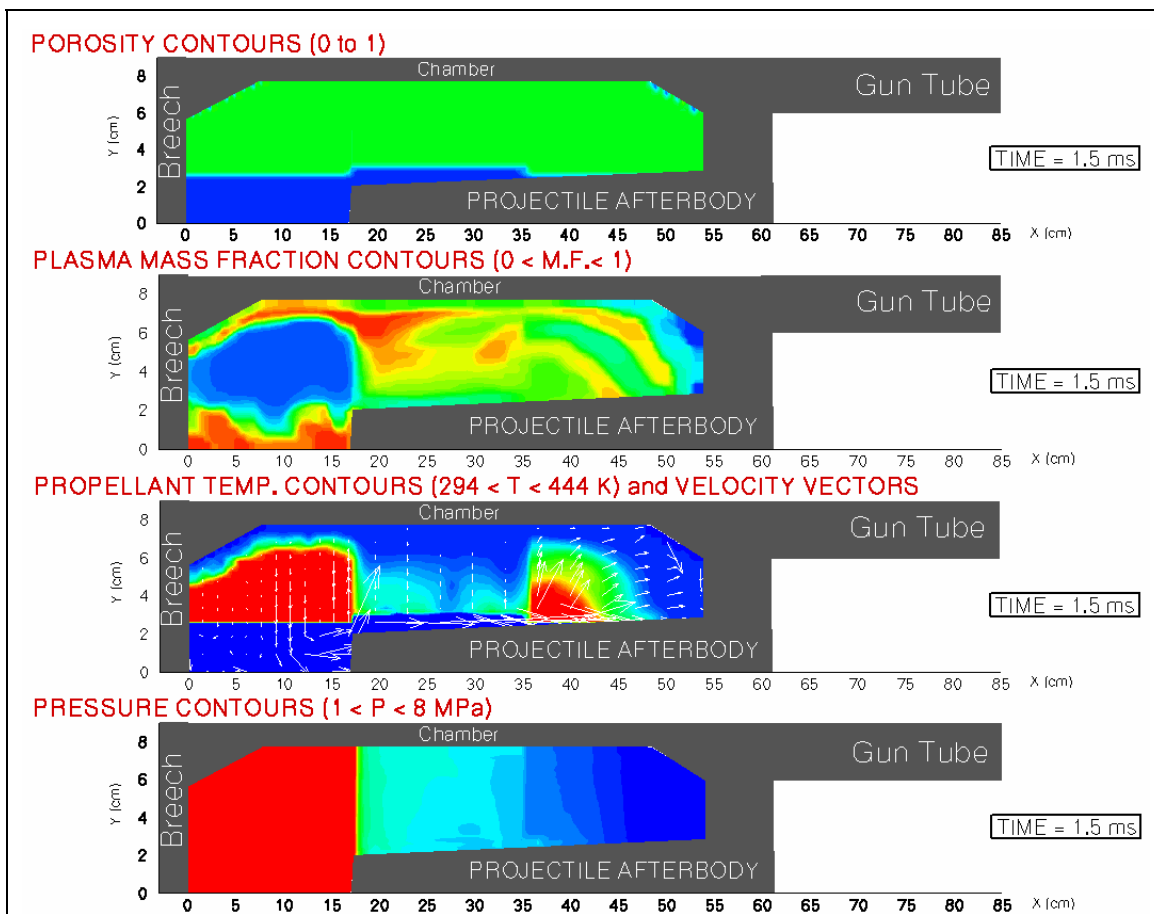


Figure 5. NGEN code results (1.5 ms since igniter function) for disk/disk/grain charge ignited using plasma.

In order to test the variability of the ignition results on the strength of the plasma igniter, the NGEN code simulations were repeated for the disk/disk/grain charge and two levels of reduced current supplied to the plasma-generating capillary. Figure 6 shows the baseline and reduced current profiles used in the present study. Results from these simulations are shown in figure 7 and compared to the result from the study using Benite igniter, originally shown in figure 3b. Reduction of the current produces a plasma pulse to the chamber that is weaker and results in an increasing longer ignition delay. It is interesting to note that a 50% reduction to the supplied current results in a situation in which the solid propellant charge fails to ignite. Of course, these results are specific to the charge being examined (i.e., the type and form function of the propellant and the loading density) as well as the plasma capillary (length, diameter, and ablative material) and the current levels. However, this results points to a potential situation in which a solid propellant charge could be designed for a particular mission but is not able to be ignited even using an ETC mechanism, pointing even more clearly to a synergism that must exist between the charge designer and the ignition system designer.

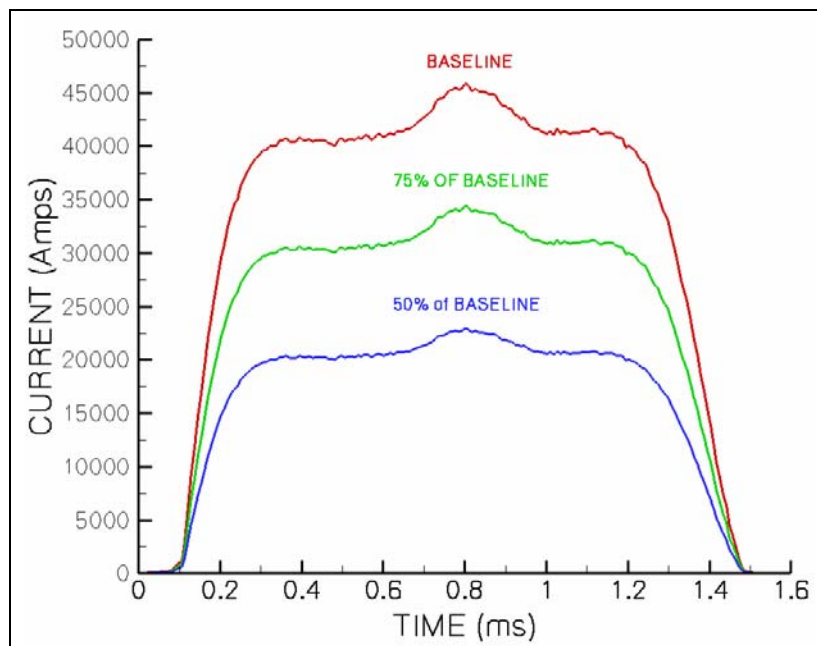


Figure 6. Current vs. time profiles used in the plasma ignition studies.

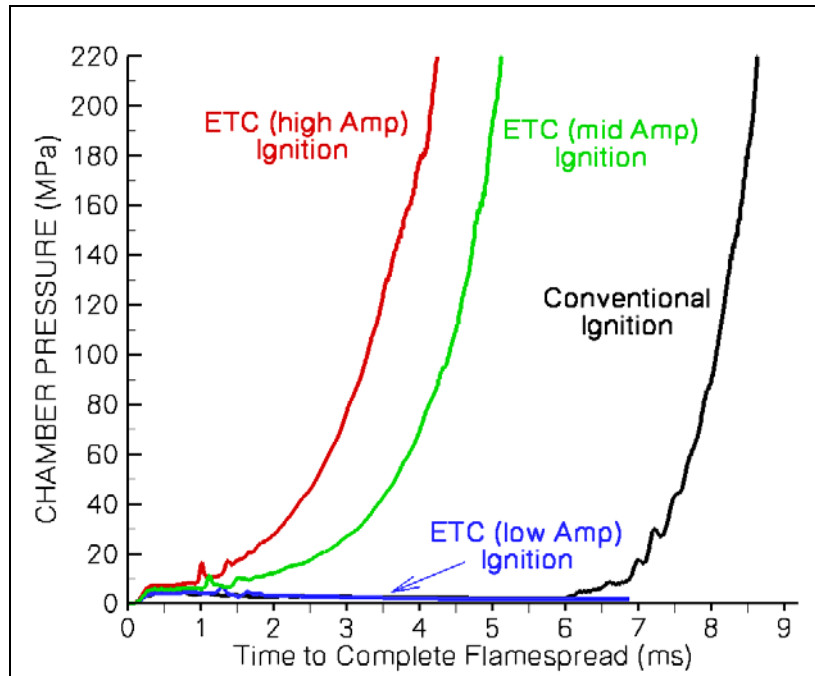


Figure 7. Chamber pressure vs. time computed using the NGEN code for the disk/disk/grain charge and using the current profiles shown in figure 6.

As these issues will be explored in future publications, the immediate question is whether the current treatment of the plasma in the NGEN code is sufficient to put confidence in the present results. There have been several previous studies in which the plasma efflux from the ETC capillary has been modeled as multicomponent (i.e., 39 chemical species), chemically reacting (i.e., 57 chemical reactions) gas (17–19). The Powell plasma capillary model (26) was employed by these studies, and as has been the case for the NGEN code, this capillary model was linked to the ARL-NSRG3 reactive flow code. These studies have pointed to the necessity of including the multicomponent nature of the plasma and its reactivity with air and propellant gases. Since a detailed chemical treatment of the plasma of this type is not compatible with the NGEN code (i.e., more of an issue with prohibitive computer run times), the subject of the remainder of this paper is an investigation of the simplified plasma representation used in the NGEN code.

4. Results for the ARL 25-mm Simulator

4.1 Description of the Simulator Experiment

The ARL 25-mm ETC ballistic simulator experiment, constructed by Chang and Howard (31–33), has been used to investigate plasma flow through the centercore of an assembly of concentric solid propellant disks that are each separated axially by a small gap—much like the configuration of an actual gun charge. Figure 8 shows a chamber, made of visually transparent



Figure 8. Photographs of the ARL 25-mm simulator loaded with disks without spacers and a single Masonite disk (dimensions shown are from Chang and Howard [32]).

acrylic, that allows cinematography of plasma flows and ignition events along the propellant bed. The chamber can withstand pressures up to ~ 7 MPa (1,000 psi) before rupture. Three Kistler pressure transducers (Model 211B1) can be installed for monitoring chamber pressures near the breech and forward ends of the chamber. The chamber is 10.15 cm long and has a 3.4-cm diameter. The chamber is narrowed to a 2.44-cm diameter at the forward end and sealed. A simulated projectile afterbody of 1.5-cm length and a 2.1-cm base diameter is inserted into the forward end of the chamber. Along the length that is of constant diameter, a series of concentric disks are placed (figure 8). These disks are made from inert material and are of 33 mm outer diameter (OD), 8-mm inner diameter (ID), and 6.35-mm thickness. Each disk is 5.84 g. In one setup, 12 disks are loaded with an initial gap between each disk of about 0.8 mm (0.030 in). In an alternate setup, 13 disks (last disk is 5.35 cm thick) are loaded with an initial gap between each disk of about 0.4 mm (0.015 in). The chamber space ahead of the last disk is filled with small seven perf grains of inert material (2.54 mm in length and 2.54 mm in diameter). A small gap of 0.076 cm exists between the breech wall and the first disk. There is a small radial gap of 0.049 cm along the radial wall of the chamber.

The ablative capillary used in this study to generate the plasma basically consists of a stainless steel cylinder that housed a polyethylene tube with an ID of 3 mm (0.125 in). A plasma injector was mounted on the breech end of the chamber. The igniter wire for the plasma was a 0.005-in-diameter nickel wire used in prior experiments. The anode was made of tungsten and with a stainless steel cathode at the plasma jet exit. The pulse power supply was capable of delivering energies of up to nearly 3 kJ at a voltage of 3 kV. A capacitor bank of 250 J and a pulse forming network delivers energy to the capillary in about 360 μ s. The voltage, current, chamber pressures, and ignition events were recorded directly on a Nicolet Integra 20 digital oscilloscope. With the measured voltage and current, the power and energy output of the capillary was subsequently calculated. These data are shown in figure 9. Typical pressure-time data recorded in the simulator are shown in figure 10.

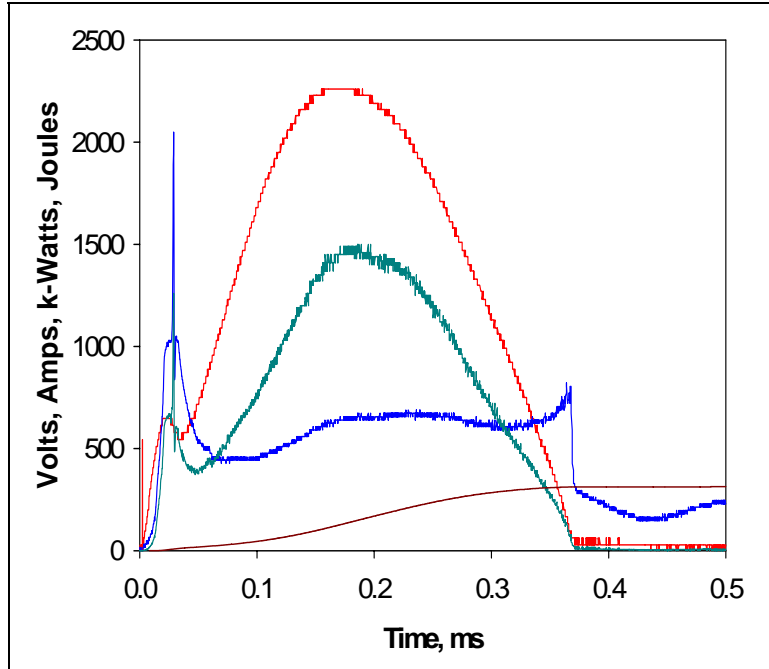


Figure 9. Electrical profiles (current in amperes: red; power in kilowatts: green; voltage in volts: blue; and energy in joules: brown) used in the ARL 25-mm simulator tests (32).

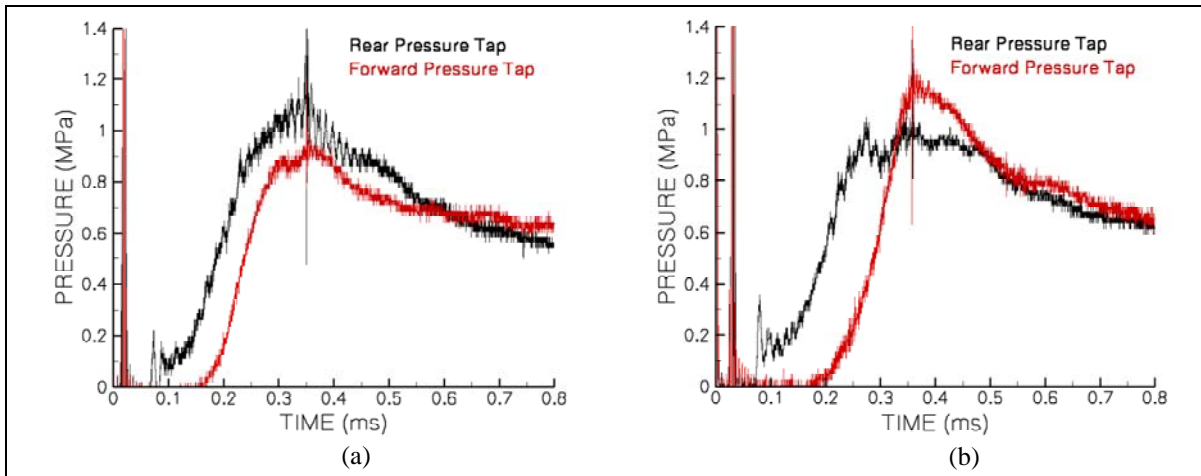


Figure 10. Pressure tap data measured in the ARL 25-mm simulator for (a) 0.015-in disk gap shown on left and (b) 0.030-in disk gap shown on right (31–33).

4.2 Description of the NGEN Code Results

Figure 11 shows a comparison between the measured and computed pressures in the 25-mm simulator loaded with disk with the 0.015-in spacers. A common color code has been used so that the pressure tap located near the breech end on the chamber is colored black and the pressure tap located in the chambrage region, loaded with the inert grains, is colored red. The NGEN simulations feature a pressure data station midway between the rear and the forward stations,

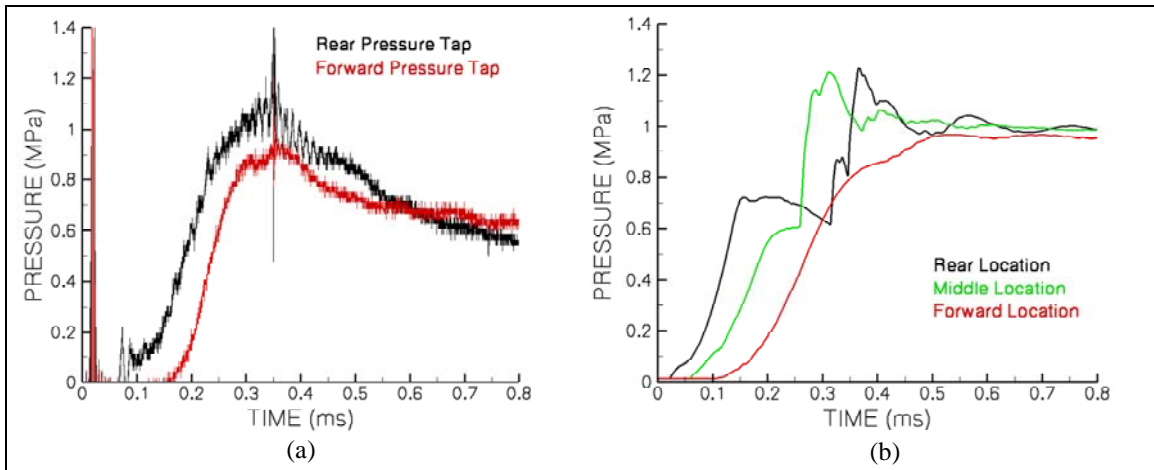


Figure 11. Pressure tap results for a disk gap of 0.015 in: (a) data measured in the ARL 25-mm simulator shown on the left and (b) NGEN code simulation shown on the right.

colored green, that was not used in the simulator. Both the measured and computed pressure for the rear location show an initial rise starting before 0.1 ms and peaking at about 0.35 ms with a pressure of about 1.1 MPa. The pressure traces for the forward location show a similar behavior with a peak of about 0.9 MPa. As is expected, each pressure tap included in the simulation is affected in turn, indicative of a pressure wave that travels through the chamber from breech end to forward chambrage; recall from figure 9 that the peak current occurs at about 0.2 ms and that the capillary is no longer charged after about 0.38 ms. While the measured data traces show a drop in pressure to a level of about 0.6 MPa after about 0.35 ms, the computations show that the pressure in the chamber, for all tap locations, reaches a steady pressure of about 1 MPa. It is thought that some loss mechanism particular to this experiment is missing from the NGEN model or that the simulator was prone to developing leaks. These issues will be resolved in future papers.

Figure 12 shows a sequence of eight color flowfield pressure maps computed as part of the NGEN simulation from 0.02 to 0.40 ms for the case of disks spaced 0.015 in apart. A constant pressure range was used for all of the plots (i.e., blue is 0.1 MPa and below, while red is 1 MPa and above). Superimposed on the pressure fields are velocity vectors shown in black, that indicate the magnitude and direction of the gas flow (note that not all vectors are plotted for clarity). The velocity vectors illustrate that the plasma efflux is emanating from a small region along the breech wall and near the chamber centerline. It can be seen that both the centercore of the chamber and the narrow space along the breech wall, that are not occupied by propellant, pressurize rapidly, followed by a pressure wave that moves from rear to forward through the disks (note the velocity vectors). When this wave reaches the base of the projectile afterbody, the chambrage region is pressurized and the wave reflects back toward the breech. By 0.40 ms, the plasma efflux has terminated, wave action has ceased, and that chamber is pressurized to near uniformity.

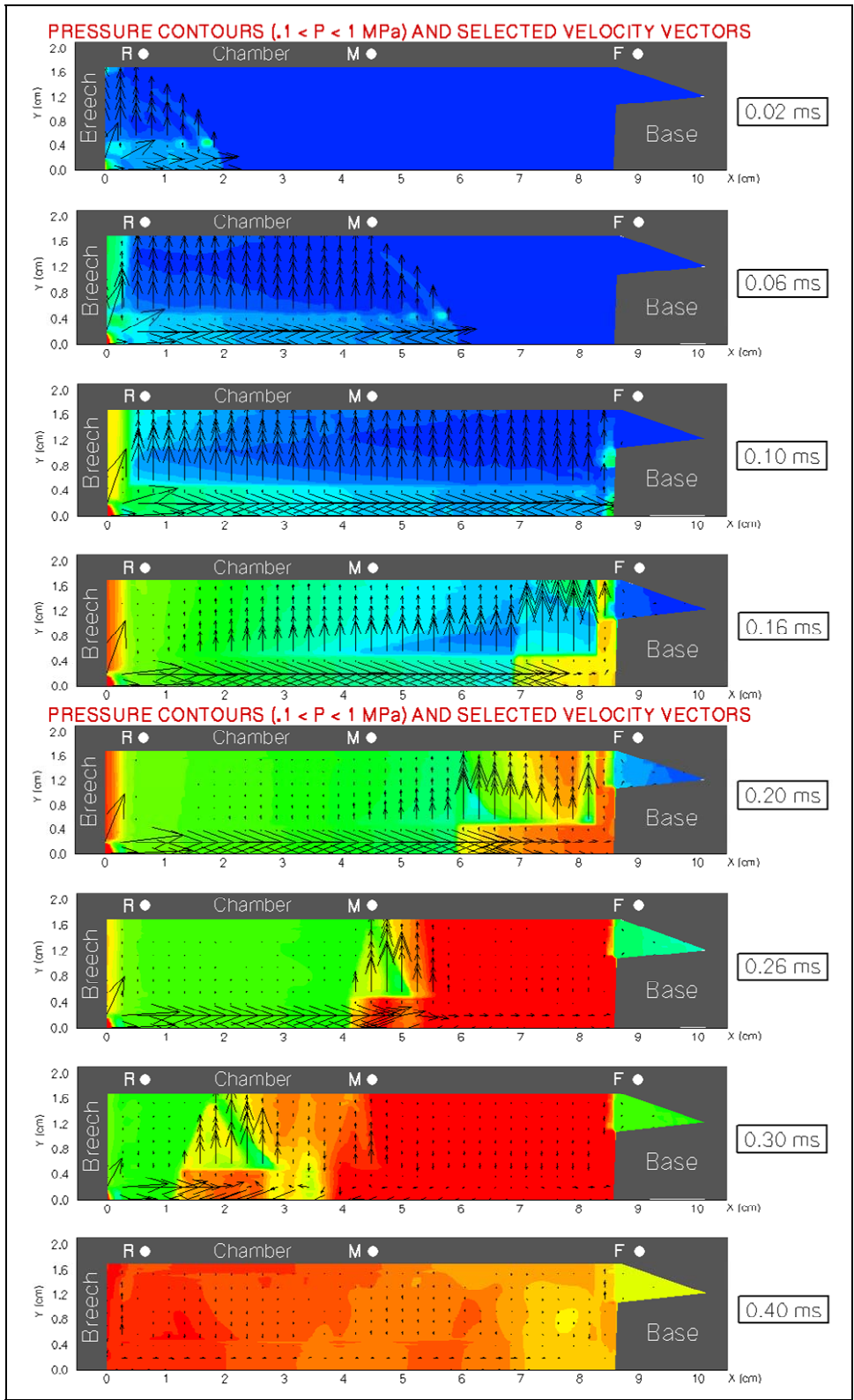


Figure 12. Color pressure contours and superimposed velocity vectors as computed using the NGEN code for disks with a gap of 0.015 in (0.4 cm) and for times from 0.02 to 0.40 ms.

Figure 13 shows a comparison between the measured and computed pressures in the 25-mm simulator loaded with disk with the 0.030-in spacers. A common color code has been used so that the pressure tap located near the breech end on the chamber is colored black and the pressure tap located in the chambrage region is colored red. The NGEN simulations also feature a pressure data station midway between the rear and the forward stations. Both the measured and computed pressures for the rear location show a rapid initial rise starting before 0.1 ms and peaking at about 0.35 ms with a pressure between 0.9 and 1.1 MPa. Due to the wider flow paths between disks in this charge, the pressure rise for the rear location is much more rapid than that seen for the small disk gap of 0.015 in (figure 11). The pressure traces for the forward location show a similar behavior with a peak of about 1.1 MPa. While the measured data traces show a drop in pressure to a level of about 0.6 MPa after about 0.35 ms, the computations show that the pressure in the chamber, for all tap locations, reaches a steady pressure of about 0.7 MPa. Due to the increased free chamber volume in this configuration, the pressure levels are slightly lower than those for the loading with a smaller disk gap. The agreement between measured and computed pressure is not as good as that reported for the propellant charge with more closely spaced disks. This discrepancy will be investigated in future papers.

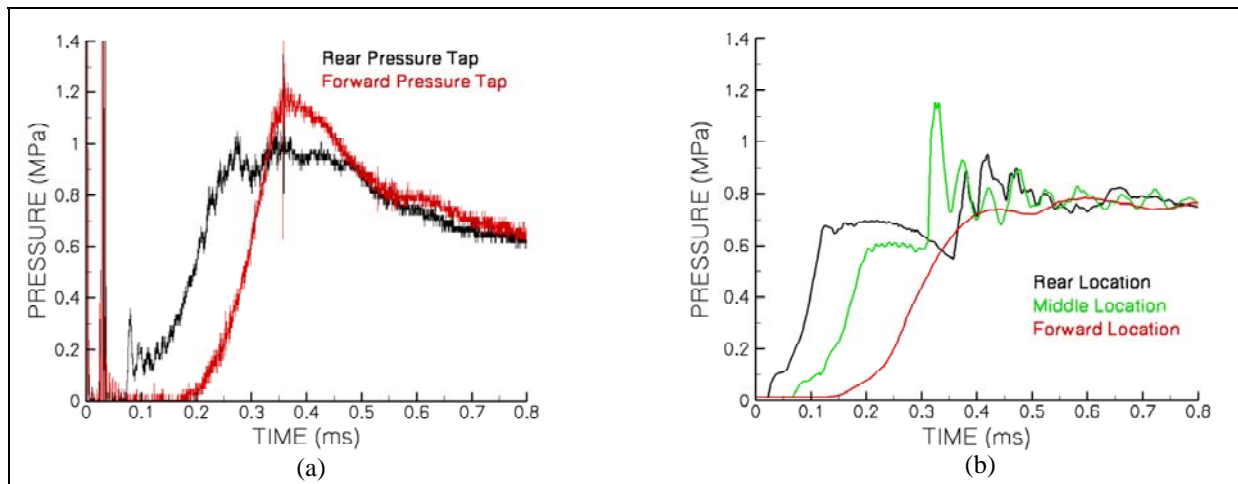


Figure 13. Pressure tap results for a disk gap of 0.030 in: (a) data measured in the ARL 25-mm simulator shown on the left and (b) NGEN code simulation shown on the right.

Figure 14 shows a sequence of eight color flowfield pressure maps computed as part of the NGEN simulation from 0.02 to 0.40 ms for the case of disks spaced 0.030 in apart. A constant pressure range was used for all of the plots (i.e., blue is 0.1 MPa and below, while red is 1 MPa and above). Superimposed on the pressure fields are velocity vectors, shown in black, that indicate the magnitude and direction of the gas flow (note that not all vectors are plotted for clarity). The velocity vectors illustrate that the plasma efflux is emanating from a small region along the breech wall and near the chamber centerline. It can be seen that both the centercore of the chamber and the narrow space along the breech wall, that are not occupied by propellant,

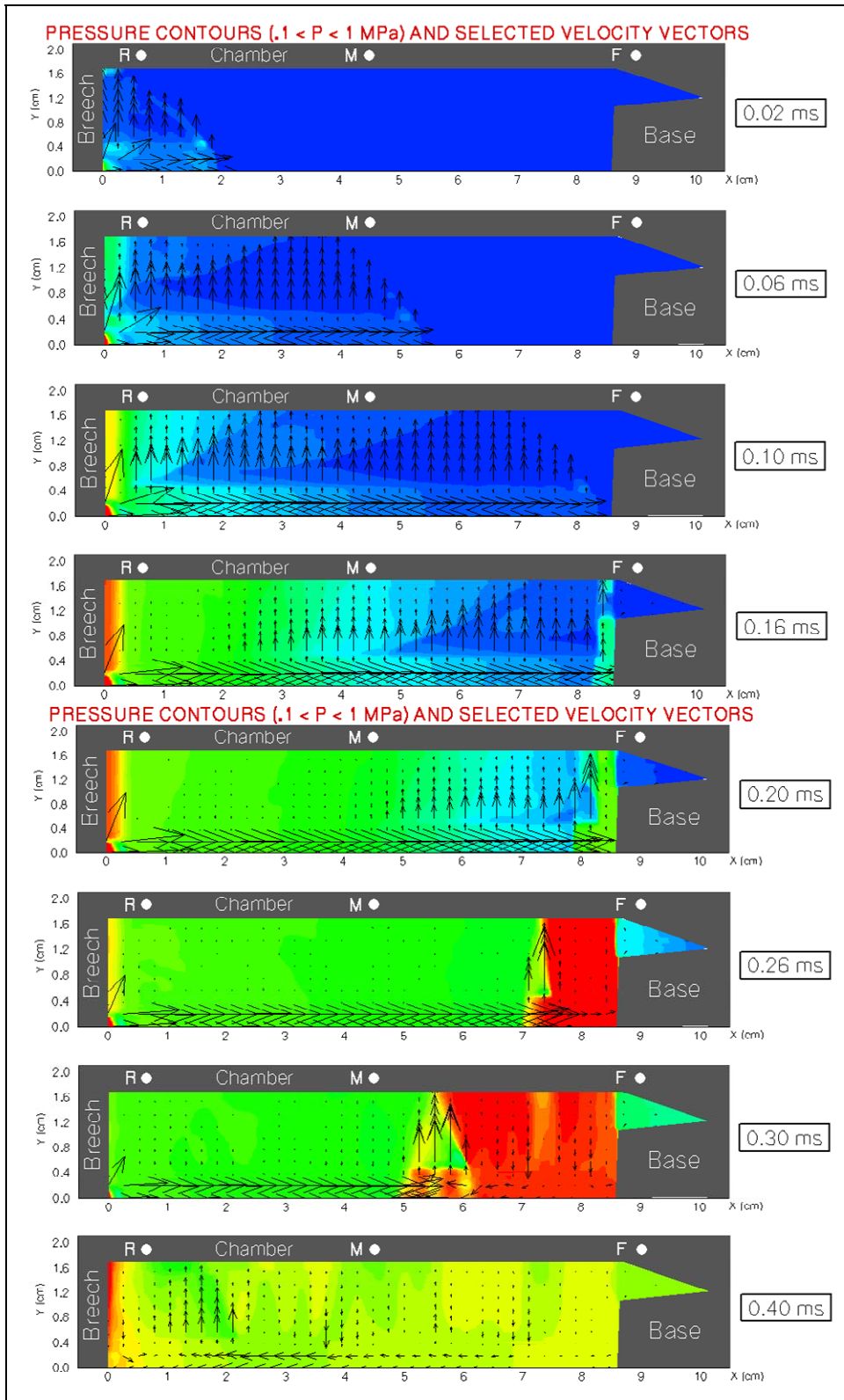


Figure 14. Color pressure contours and superimposed velocity vectors as computed using the NGEN code for disks with a gap of 0.030 in (0.8 cm) and for times from 0.02 to 0.40 ms.

pressurize rapidly, followed by a pressure wave that moves from rear to forward through the disks (note the velocity vectors). When this wave reaches the base of the projectile afterbody, the chambrage region is pressurized and the wave reflects back toward the breech. Both the speed of this advancing pressure wave and the magnitude of the wave reflection are slower and weaker, respectively, than those for the configuration with a smaller gap between disks which corresponds to the increased free chamber volume resulting from the wider gaps between disks. By 0.40 ms, the plasma efflux has terminated, wave action has ceased and that chamber is pressurized to near uniformity but to a lower level than that for the disk gap of 0.015 in (recall figure 12).

4.3 Sensitivity Study for the NGEN Code Results

Since the results of a flow field simulation are often dependent on the resolution of the computational grid (or mesh), a grid study was conducted for the present simulations. Experience with the NGEN code has shown that grid dependence is very mild for typical gun chamber configurations especially when the charge is purely granular. In the present case, the outer diameter of the disks does not match the chamber diameter and thus a small flow gap (0.049 cm) is present along the radial wall of the chamber. The radial grid for the present simulations was constructed in order to capture this radial gap with one grid cell. The radial grid consists of 53 cells (i.e., uniform radial spacing of 0.032 cm). In addition, there exists a small axial gap (0.076 cm) between the chamber breech wall and the surface of the first disk. Gaps between the disks were either 0.038 cm (0.015 in) or 0.076 cm (0.030 in). Since the NGEN code takes a macroscopic approach to the representation of the disk propellant region, the individual gaps between disks are not explicitly represented even though the gap between the breech wall and the first disk can be explicitly represented. For numerical stability and accuracy considerations, it is desirable to distribute the axial grid in a uniform manner, consistent with the radial grid. In order to capture the axial wall gap, 230 axial cells are required in the constant diameter section of the chamber. Two additional axial grids were constructed of 58 and 29 axial cells in the constant diameter section of the chamber. For the entire chamber (i.e., including the chambrage section) the course mesh {axial, radial} is {34, 53}, the fine mesh is {68, 53}, and the finer mesh is {250, 53}.

Figures 15–17 show the NGEN code pressure-time results for the three computational meshes, previously discussed, referring to the rear, middle, and forward pressure data collection points. The same color code has been maintained as was used in figures 11 and 13 in which the finer grid was used to generate results. In general and across the pressure data locations and disk gaps, the final pressure computed at about 0.8 ms was independent of the computational mesh, as expected. For the rear pressure collection location, the NGEN code showed markedly higher pressures for the courser meshes. In fact, the pressure computed using the finer mesh agreed closer with the measured data (recall figures 11 and 13). For the middle pressure collection location, the NGEN code showed the least dependence on computational mesh used. For the forward pressure collection location that is actually in the region occupied by granular

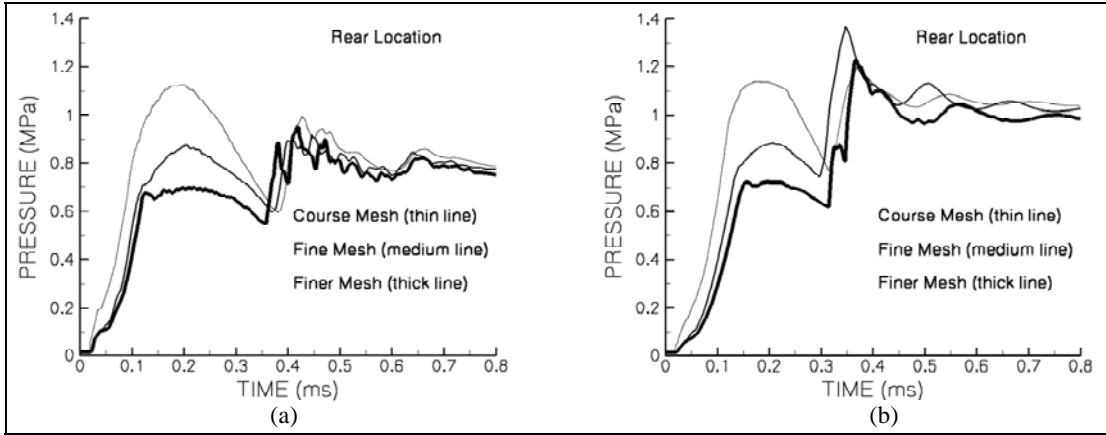


Figure 15. NGEN code computed pressure results for the rear location using several levels of computational mesh resolution: (a) 0.015-in disk gap and (b) 0.030-in disk gap.

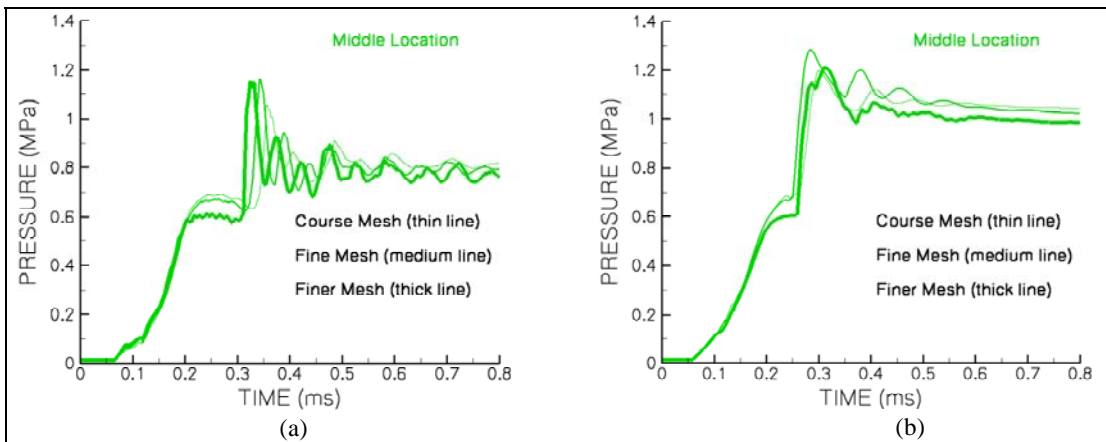


Figure 16. NGEN code computed pressure results for the middle location using several levels of computational mesh resolution: (a) 0.015-in disk gap and (b) 0.030-in disk gap.

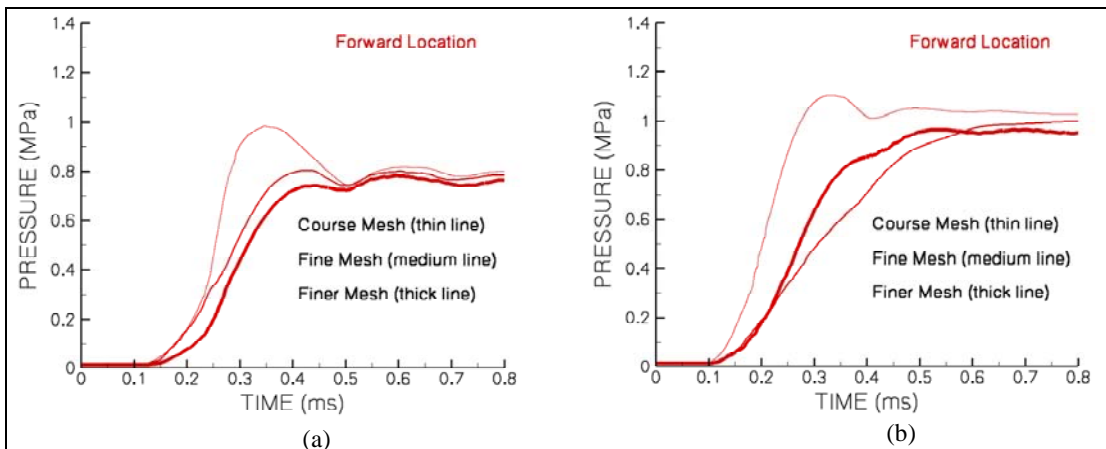


Figure 17. NGEN code computed pressure results for the forward location using several levels of computational mesh resolution: (a) 0.030-in disk gap and (b) 0.015-in disk gap.

propellant, the NGEN code showed the most dependence on computational mesh used, the results for the finer mesh agreeing best with the measured data. Overall, it has been shown that a very fine mesh would need to be used in the NGEN simulation for disk propellant. Subsequent NGEN simulations using a still finer mesh did not yield pressure-time results significantly different than those shown for the “finer” mesh, previously discussed.

5. Summary and Conclusions

The NGEN multidimensional, multiphase CFD code has been successfully used to model the interior ballistics of solid propellant charges ignited using hot chemical gases like those generated by burning Benite. In order to model charges ignited using injected plasma, which is generated by an ablation capillary of polyethylene, the NGEN code was upgraded with a single-component, nonreacting gas phase treatment of the plasma and linked to a well-known and independently validated capillary model. When applied to the simulation of tightly packed solid propellant charges, the NGEN code shows that the plasma ignition is much more prompt when compared to the Benite igniter. This result is in agreement with gun firing data. Further, the NGEN simulations show that the ignition delay is lengthened, perhaps to the point of a nonignition event, when the current that is input to the ablation capillary is reduced. This is an important result as it necessitates a closer linkage between the charge designer and the igniter designer when the ETC option is utilized. Given independent plasma-propellant modeling results that point to the need for a multicomponent, reacting flow representation of the plasma and the incompatibility of this level of plasma modeling with the NGEN code, within the constraints of currently available computers, there is an immediate need to validate the NGEN code for the design of ETC guns. The first step in this effort has been to compare the chamber pressure measured in a ballistics simulator with that computed using the code. The configuration chosen was a 25-mm chamber filled with inert disks and linked to an ablative capillary of the size and power of a typical ETC gun igniter. Preliminary results for the use of two different disk spacers look very encouraging. The need for an appropriately refined computational mesh was highlighted. Future work is required that will examine the repeatability of the data and extend the comparison of the NGEN model and the ballistics simulator.

6. References

1. Del Güercio, M. Propellant Burn Rate Modification by Plasma Injection. *Proceedings of the 34th JANNAF Combustion Meeting, CPIA Publication 662*, October 1997; Vol. 1, pp 35–42.
2. Perelmutter, L.; Sudai, M.; Goldenberg, C.; Kimhe, D.; Zeevi, Z.; Arie, S.; Melnik, M.; Melnik, D. Temperature Compensation by Controlled Ignition Power in SPETC Guns. *Proceedings of the 16th International Symposium on Ballistics*, September 1996, pp 145–152,
3. Dyvik, J. A.; Katulka, G. ETC Temperature Compensation; Experimental Results of 120-mm Test Firings. *Proceedings of the 33rd JANNAF Combustion Meeting, CPIA Publication 653*, November 1996; Vol. 3, pp 111–119.
4. Katulka, G. L.; Dyvik, J. Experimental Results of Electrical Plasma Ignition in 120-mm Solid Propellant Tank Gun Firings. *Proceedings of the 33rd JANNAF Combustion Meeting, CPIA Publication 653*, November 1996; Vol. 3, pp 103–110.
5. White, K. J.; Katulka, G. L.; Khuan, T.; Nekula, K. *Plasma Characterization for Electrothermal-Chemical (ETC) Gun Applications*; ARL-TR-1491; U.S. Army Research Laboratory: Aberdeen Proving Ground, MD, September 1997.
6. Perelmutter, L.; Goldenberg, C.; Sudai, M.; Alimi, R.; Furman, M.; Kimhe, D.; Appelbaum, G.; Arie, S.; Zeevi, Z.; Melnik, D. Experimental Study of Plasma Propagation and Ignition of Solid Propellant in a Gun Chamber. *Proceedings of the 16th International Symposium on Ballistics*, September 1996.
7. Nusca, M. J.; White, K. J. Plasma Radiative and Convective Interactions with Propellant Beds. *Proceedings of the 34th JANNAF Combustion Meeting, CPIA Publication 662*, October 1997; Vol. 1, pp 21–42.
8. White, K. J.; Williams, A. W.; Nusca, M. J. Plasma Output and Propellant Radiation Absorption Characteristics. *Proceedings 35th JANNAF Combustion Meeting, CPIA Publication 680*, December 1998; Vol. 1, pp 237–246.
9. Kaste, P. J.; Birk, A.; Del Güercio, M. A.; Lieb, R.; Kinkennon, A. *Surface Phenomena of Plasma-Treated Propellant Samples*; ARL-TR-2500; U.S. Army Research Laboratory: Aberdeen Proving Ground, MD, May 2001.

10. Williams, A. W.; White, K. J. Plasma-Propellant Interaction Studies: Measurements of In-Depth Propellant Heating by Plasma Radiation; Investigation of Possible Plasma-Induced Propellant Erosion. *Proceedings of the 36th JANNAF Combustion Meeting, CPIA Publication 691*, October 1999; Vol. 2, pp 67–76.
11. Beyer, R. A. Small Scale Experiments in Plasma Propellant Interactions. *Proceedings of the 37th JANNAF Combustion Subcommittee Meeting, CPIA Publication 701*, November 2000; Vol. 1, pp 137–144.
12. Fifer, R. A.; Sagan, E. S.; Beyer, R. A. Investigation of the Role of Plasma Chemistry in the Plasma Propellant Interaction Process. Proceedings of the 38th JANNAF Combustion Subcommittee Meeting, Eglin Air Force Base, FL, April 2002.
13. Litzinger, T. A.; Li, J-Q.; Kwon, J.; Thynell, S. Experimental Investigations of the Characteristics of Electrothermal-Chemical Plasma. Proceedings of the 38th JANNAF Combustion Subcommittee Meeting, Eglin Air Force Base, FL, April 2002.
14. Chang, L-M.; Beyer, R. A.; Howard, S. L. Characterization of Plasma Jet Flows and their Interaction with Propelling Charges. Proceedings of the 38th JANNAF Combustion Subcommittee Meeting, Eglin Air Force Base, FL, April 2002.
15. McQuaid, M. J.; Nusca, M. J. *Calculating the Chemical Compositions of Plasmas Generated by an Ablating-Capillary Arc Ignition System*; ARL-TR-2046; U.S. Army Research Laboratory: Aberdeen Proving Ground, MD, 1999.
16. McQuaid, M. J.; Nusca, M. J. *Thermodynamic Property Characterization of Plasmas Generated by an Ablating-Capillary Arc*; ARL-TR-2427; U.S. Army Research Laboratory: Aberdeen Proving Ground, MD, May 2001.
17. Nusca, M. J.; McQuaid, M. J.; Anderson, W. R. Numerical Model of the Plasma Jet Generated by an Electrothermal-Chemical Igniter. *Journal of Thermophysics and Heat Transfer* **January–March 2002**, 16 (1), 44–52.
18. Nusca, M. J.; Anderson, W. R.; McQuaid, M. J. *Multispecies Reacting Flow Model for the Plasma Efflux of an ETC Igniter – Application to an Open-Air Plasma Jet Impinging on an Instrumented Probe*; ARL-TR-3227; U.S. Army Research Laboratory: Aberdeen Proving Ground, MD, July 2004.
19. Nusca, M. J.; Anderson, W. R.; McQuaid, M. J. *Multispecies Reacting Flow Model for the Plasma Efflux of an ETC Igniter – Application to an Open-Air Plasma Jet Impinging on an Instrumented Plate*; ARL-TR-3275; U.S. Army Research Laboratory: Aberdeen Proving Ground, MD, August 2004.

20. Anderson, W. R.; Schroeder, M. A. Chemical Mechanism for ETC Plasma Interaction with Air. *Proceedings of the 36th JANNAF Combustion Meeting, CPIA Publication 691*, October 1999; Vol. 2, pp 43–54.
21. Gough, P. S.; Modeling Arbitrarily Packaged Multi-Increment Solid Propellant Charges of Various Propellant Configurations. *Proceedings of the 33rd JANNAF Combustion Meeting, CPIA Publication 653*, November 1996; Vol. 1, pp 421–435.
22. Gough, P. S. Extensions to the NGEN Code: Propellant Rheology and Container Properties. *Proceedings of the 34th JANNAF Combustion Meeting, CPIA Publication 662*, Vol. 3, October 1997, pp 265–281.
23. Nusca, M. J.; Gough, P. S. *Numerical Model of Multiphase Flows Applied to Solid Propellant Combustion in Gun Systems*; AIAA Paper No. 98-3695, July 1998.
24. Nusca, M. J. *High-Performance Computing and Simulation for Advanced Armament Propulsion*; ARL-TR-3215; U.S. Army Research Laboratory: Aberdeen Proving Ground, MD, June 2004.
25. Boris, J. P.; Landsberg, A. M.; Oran, E. S.; Gardner, J. H. *LCPFCT – A Flux-Corrected Transport Algorithm for Solving Generalized Continuity Equations*; NRL-MR/6410-93-7192; U.S. Naval Research Laboratory: Washington, DC, April 1993.
26. Powell, J. D.; Zielinski, A. E. *Theory and Experiment for an Ablating-Capillary Discharge and Application to Electrothermal-Chemical Guns*; BRL-TR-3355; U.S. Army Ballistic Research Laboratory: Aberdeen Proving Ground, MD, 1992.
27. Conroy, P. J.; Nusca, M. J. *Progress in the Modeling of High-Loading Density Direct-Fire Charges Using the NGEN Multiphase CFD Code*; ARL-TR-2934; U.S. Army Research Laboratory: Aberdeen Proving Ground, MD, March 2003.
28. Nusca, M. J. Numerical Simulation of Plasma Ignition for High-Loading Density Charges in an ETC Sun Using the NGEN Code. *Proceedings of the 39th JANNAF Combustion Meeting, CPIA Publication JSC CD-25*, 2003.
29. Anderson, R.; Fickie, K. *IBHGV2 – A User’s Guide*; BRL-TR-2829; U.S. Army Ballistic Research Laboratory: Aberdeen Proving Ground, MD, July 1987.
30. Gough, P. S. *Interior Ballistics Modeling: Extensions to the XKTC Code and Analytical Studies of Pressure Gradient for Lumped Parameter Codes*; ARL-CR-460; U.S. Army Research Laboratory: Aberdeen Proving Ground, MD, February 2001.
31. Chang, L. M. *Interior Ballistic Simulations of 25-mm Gun Charges*; BRL-TR-3330; U.S. Army Ballistic Research Laboratory: Aberdeen Proving Ground, MD, 1992.

32. Chang, L. M.; Howard, S. L. Characterization of Plasma Jet Flows and Their Interaction With Propelling Charges. Proceedings of 20th International Symposium on Ballistics, Orlando, FL, September 2002.
33. Chang, L. M.; Howard, S. L. Characterization of Flame Propagation in Narrow Channels of Disc Propellant Charges with Plasma Ignition. *Proceedings of the 51st JANNAF Propulsion Meeting, CPIA Publication JPMCD02*, November 2002.

NO. OF
COPIES ORGANIZATION

1 DEFENSE TECHNICAL
(PDF INFORMATION CTR
ONLY) DTIC OCA
8725 JOHN J KINGMAN RD
STE 0944
FORT BELVOIR VA 22060-6218

1 US ARMY RSRCH DEV &
ENGRG CMD
SYSTEMS OF SYSTEMS
INTEGRATION
AMSRD SS T
6000 6TH ST STE 100
FORT BELVOIR VA 22060-5608

1 INST FOR ADVNCD TCHNLGY
THE UNIV OF TEXAS
AT AUSTIN
3925 W BRAKER LN
AUSTIN TX 78759-5316

1 DIRECTOR
US ARMY RESEARCH LAB
IMNE ALC IMS
2800 POWDER MILL RD
ADELPHI MD 20783-1197

3 DIRECTOR
US ARMY RESEARCH LAB
AMSRD ARL CI OK TL
2800 POWDER MILL RD
ADELPHI MD 20783-1197

ABERDEEN PROVING GROUND

1 DIR USARL
AMSRD ARL CI OK TP (BLDG 4600)

NO. OF
COPIES ORGANIZATION

1 DIRECTOR
US ARMY RESEARCH LAB
AMSRD ARL D
J MILLER
2800 POWDER MILL RD
ADELPHI MD 20783-1197

3 DIRECTOR
US ARMY RESEARCH LAB
AMSRD ARL RO P
D MANN
R SHAW
TECH LIB
PO BOX 12211
RESEARCH TRIANGLE PARK NC
27709-2211

8 US ARMY AVIATN & MSLE CMD
AMSRD AMR PS PT
W CHEW
C DOLBEER
J S LILLY
M LYON
J M FISHER
B P MARSH
R S MICHAELS
D THOMPSON
REDSTONE ARSENAL AL
35898-5249

2 PM MAS
SFAE AMO MAS
LTC M BUTLER
PICATINNY ARSENAL NJ
07806-5000

2 PM CAS
SFAE AMO CAS
PICATINNY ARSENAL NJ
07806-5000

8 DIR BENET WEAPONS LAB
M AUDINO
R DILLON
R FISCELLA
R HASENBEIN
E KATHE
J MCNEIL
K MINER
S SOPOK
WATERVLIET NY 12189-4000

NO. OF
COPIES ORGANIZATION

17 CDR US ARMY ARDEC
D CARLUCCI
R CARR
R CIRINCIONE
S EINSTEIN
T GORA
P HUI
J LANNON
E LOGSDEN
P LU
B MACHAK
S NICHOLICH
P O'REILLY
J O'REILLY
J RUTKOWSKI
A SABASTO
J SHIN
R SURAPANENI
PICATINNY ARSENAL NJ 07806-5000

1 CDR
RADFORD ARMY AMMO PLANT
SMCAR QA HI LIB
RADFORD VA 24141-0298

1 COMMANDANT
USAFC&S
ATSF CN P GROSS
FT SILL OK 73503-5600

2 CDR NAVAL RSRCH LAB
TECH LIBRARY
J BORIS
WASHINGTON DC 20375-5000

1 OFFICE OF NAVAL RSRCH
J GOLDWASSER
875 N RANDOLPH ST RM 653
ARLINGTON VA 22203-1927

6 CDR
NAVAL SURFACE WARFARE CTR
R2A R DOHERTY
TM3 C GOTZMER
R22 C MICHIZENZI
OPA S MITCHELL
R3A S C SMITH
TECHLIB
INDIAN HEAD MD 20640-5000

NO. OF
COPIES ORGANIZATION

5 CDR
NAVAL SURFACE WARFARE CTR
J FRAYSEE G33
R FRANCIS T08
T C SMITH
T TSCHIRN G30
TECHLIB
DAHLGREN VA 22448-5000

3 CDR
NAVAL AIR WARFARE CTR
A ATWOOD
S BLASHILL
T PARR
CHINA LAKE CA 93555-6001

1 AIR FORCE RSRCH LAB
MNME EN MAT BR
B WILSON
2306 PERIMETER RD
EGLIN AFB FL 32542-5910

1 AIR FORCE OFC OF SCI RSRCH
M BERMAN
875 N RANDOLPH ST
STE 235 RM 3112
ARLINGTON VA 22203-1768

1 NASA LANGLEY RSRCH CENTER
D BUSHNELL
MS 110
HAMPTON VA 23681-2199

1 DIR SANDIA NATL LABS
M BAER DEPT 1512
PO BOX 5800
ALBUQUERQUE NM 87185

2 DIR LAWRENCE LIVERMORE NL
L FRIED
M MURPHY
PO BOX 808
LIVERMORE CA 94550-0622

1 CENTRAL INTELLIGENCE AGENCY
J BACKOFEN
RM 4PO7 NHB
WASHINGTON DC 20505

1 BATTELLE EAST SCI & TECH
A ELLIS
1204 TECHNOLOGY DR
ABERDEEN MD 21001-1228

NO. OF
COPIES ORGANIZATION

2 JHU CHEM PROP INFO AGENCY
W HUFFERD
R FRY
10630 LITTLE PATUXENT PKWY
STE 202
COLUMBIA MD 21044-3200

1 OUSD (AT&L)/STRAT & TACT
SYS MUNITIONS
T MELITA
3090 DEFENSE PENTAGON
RM 3B1060
WASHINGTON DC 20301-3090

1 BRIGHAM YOUNG UNIV
DEPT OF CHEMICAL ENGRG
M BECKSTEAD
PROVO UT 84601

1 CALIF INSTITUTE OF TECHLGY
F E C CULICK
204 KARMAN LAB
MS 301 46
1201 E CALIFORNIA ST
PASADENA CA 91109

2 UNIV OF ILLINOIS
DEPT OF MECH INDUSTRY
ENGINEERING
H KRIER
R BEDDINI
144 MEB 1206 N GREEN ST
URBANA IL 61801-2978

5 PENNSYLVANIA STATE UNIV
DEPT OF MECHANICAL ENGRG
K KUO
T LITZINGER
G SETTLES
S THYNELL
V YANG
UNIVERSITY PARK PA 16802-7501

<u>NO. OF COPIES</u>	<u>ORGANIZATION</u>
1	ARROW TECHLGY ASSOC INC 1233 SHELBURNE RD D 8 SOUTH BURUNGTION VT 05403
1	ALLEGHENY BALLISTICS LAB PO BOX 210 ROCKET CENTER WV 26726
1	ATK ORDNANCE 4700 NATHAN LANE PLYMOUTH MN 55442
3	ATK AMMO & ENERGETICS D A WORRELL W J WORRELL S RITCHIE RADFORD ARMY AMMO PLANT ROUTE 114 PO BOX 1 RADFORD VA 24141-0299
4	ATK THIOKOL P BRAITHWAITE T B FARABAUGH W B WALKUP R WARDLE PO BOX 707 BRIGHAM CITY UT 84302-0707
1	ATK ELKTON J HARTWELL PO BOX 241 ELKTON MD 21921-0241
1	BAE ARMAMENT SYS DIV JAHN DYVIK 4800 E RIVER RD MINNEAPOLIS MN 55421-1498
2	GEN DYNAMICS ORD/TACT SYS N HYLTON J BUZZETT 10101 DR M L KING ST N ST PETERSBURG FL 33716
3	GENERAL DYNAMICS ST MARKS J DRUMMOND H RAINES D W WORTHINGTON PO BOX 222 SAINT MARKS FL 32355-0222

<u>NO. OF COPIES</u>	<u>ORGANIZATION</u>
1	GENERAL DYNAMICS ARM SYS J TALLEY 128 LAKESIDE AVE BURLINGTON VT 05401
1	HICKS AND ASSOCIATES SAIC I MAY 7990 SCIENCE APPLIC CT VIENNA VA 22182
1	PAUL GOUGH ASSOC INC P S GOUGH 1048 SOUTH ST PORTSMOUTH NH 03801-5423
3	VERITAY TECHGY INC R SALIZONI J BARNES E FISHER 4845 MILLERSPORT HWY EAST AMHERST NY 14501-0305
1	SRI INTERNATIONAL PROPULSION SCIENCES DIV TECH LIB 333 RAVENWOOD AVE MENLO PARK CA 94025-3493
1	NETWORKING COMPUTING SVCS S RAY 1200 WASHINGTON AVE S MINNEAPOLIS MN 55415

NO. OF
COPIES ORGANIZATION

ABERDEEN PROVING GROUND

66 DIR USARL
AMSRD ARL WM
T ROSENBERGER
AMSRD ARL WM M
S MCKNIGHT
AMSRD ARL WM T
B BURNS
AMSRD ARL WM TB
P BAKER
AMSRD ARL WM B
C CANDLAND
J MORRIS
J NEWILL
M ZOLTOSKI
AMSRD ARL WM BA
B DAVIS
G BROWN
D HEPNER
G KATULKA
T KOGLER
D LYON
AMSRD ARL WM BC
M BUNDY
G COOPER
J DESPIRITO
J GARNER
P PLOSTINS
J SAHU
S SILTON
P WEINACHT
AMSRD ARL WM BD
W ANDERSON
R BEYER
A BRANT
S BUNTE
L CHANG
T COFFEE
J COLBURN
P CONROY
N ELDREDGE
B FORCH
B HOMAN
A HORST
S HOWARD (6 CPS)
P KASTE
A KOTLAR
C LEVERITT
R LIEB
K MCNESBY
M MCQUAID
A MIZIOLEK
J NEWBERRY

NO. OF
COPIES ORGANIZATION

M NUSCA (6 CPS)
R PESCE-RODRIGUEZ
S PIRIANO
G REEVES
B RICE
R SAUSA
J SCHMIDT
A WILLIAMS
AMSRD ARL WM BF
R ANDERSON
W OBERLE
D WILKERSON
AMSRD ARL WM EG
E SCHMIDT
AMSRD ARL WM SG
W CIEPIELA

1 CDR USAATC
CSTE DTC AT SL
APG MD 21005